Deuteron structure and form factors: Using an inverse potential approach

Anil Khachi[1], Lalit Kumar[1], M. R. Ganesh Kumar[2], and O. S. K. S. Sastri[1,*]

[1]*Department of Physics and Astronomical Sciences, Central University of Himachal Pradesh, Dharamshala, Himachal Pradesh 176215, India*

[2]*Applied Materials India Private Limited, Bengaluru 560066, India*

(Received 16 January 2023; revised 13 April 2023; accepted 5 June 2023; published 28 June 2023)

Background: The ground-state wave function of deuteron is required to obtain its structure and form factors. Currently, an accurate analytical expression for the wave function is not available.

Purpose: In this paper, we determine the deuteron's static properties, low-energy scattering parameters, and form factors using an analytical ground-state wave function.

Methods: An inverse S-wave potential is constructed using the Morse function as the zeroth reference potential. The scattering phase shifts (SPSs) at different laboratory energies are determined using phase function method. The model parameters are optimized using least-squares minimization by both global optimization and combinatorial data analysis techniques.

Results: The mean absolute error between experimental and obtained SPSs for the state $^3S_1$, using global optimization, is found to be 0.35. The low-energy scattering parameters match well with the expected values. The analytical ground-state deuteron wave function (DWF) is obtained by utilizing the experimental value for the quadrupole moment. Other static properties and form factors determined from the obtained DWF are found to be in close agreement with experimental ones.

Conclusions: Modeling np interaction using the Morse potential has been reasonably successful in explaining all static and low-energy parameters as well as SPSs for laboratory energies up to 350 MeV. The obtained electromagnetic form factors using an analytical deuteron ground-state wave function are found to closely match with experimental data.

DOI: 10.1103/PhysRevC.107.064002

I. INTRODUCTION

Study of the deuteron to understand its experimentally observed static properties has been reviewed by Zhaba [1] and Garcon and Van Orden [2]. The best results are from nucleon-nucleon (NN) interaction precision potentials [3–8] and those obtained with chiral perturbation theory [9]. All these describe the NN interaction as consisting of long-range one-pion exchange (OPE). The intermediate- and short-range interactions are modeled using either simple functional forms [7] or meson exchanges [8]. At very short internucleon distances, a strong repulsive core is expected due to strong anticorrelation between nucleons. This is modeled phenomenologically using exponential functions. Finally, model parameters are obtained by directly fitting experimental scattering phase shifts (SPSs) for various ℓ channels. Two reviews of these realistic potentials by Naghdi [10] and Machleidt [11] point out that these precision potentials with very different theoretical considerations give rise to practical utility in nuclear structure calculations even though they have very different shapes for nuclear interaction potential. For example, while SPS predictions for $^3S_1$ and $^1S_0$ due to precision potentials are indistinguishable, their corresponding potentials are entirely different due to different mathematical forms [12].

The first phenomenological potential for np interaction, by Yukawa *et al.* [13], suggests an attractive nature and successfully obtains SPSs for laboratory energies up to 50 MeV. This potential is modified by Malfliet-Tjon [14] by adding a repulsive term similar to Yukawa et al.'s [13] form. This gives a good match of the observed SPSs for energies up to 350 MeV, but does not give an accurate binding energy for the deuteron. Also, it does not have an analytical solution for its corresponding time-independent Schrödinger equation (TISE). On the other hand, the Hulthen [15] and Manning-Rosen [16] potentials suggest an attractive nature for np interaction and have analytical solutions that give rise to accurate binding energy but do not correctly predict the observed SPSs. All these indicate a need for a phenomenological potential that can explain the observed SPSs for all energies up to 350 MeV, accurately obtain the binding energy of a deuteron, and preferably has an analytical solution to the TISE.

The need for an analytical deuteron wave function (DWF) for calculation of the deuteron's polarization characteristics has been emphasized by Zhaba [1] in his review. Garcon and Van Orden [2] have pointed out that one of the conspicuous features of np interaction is its short-range repulsion. This is the reason the Argonne v_{18} potential has a dip in its ground-state radial wave function at small r, which results in a node in its corresponding momentum wave function. An analytical solution for $^3S_1$ could further confirm the nature of such behavior seen at short distances.

*Corresponding author: sastri.osks@hpcu.ac.in

Recently, an effective potential and a ground-state wave function [17] for deuterons have been obtained by employing a supersymmetric (SUSY) quantum mechanics approach, where the D-state wave function is taken to be proportional to that of the S state. We have utilized the Morse function as in Refs. [18,19] to guide the construction of inverse potentials [20,21]. Considering the available experimental data, model parameters of the Morse potential have been obtained based on a global optimization algorithm (GOA). This amounts to building model from data as in physics-based machine learning, wherein the number of data points being used for optimization is much larger than the number of model parameters. This approach is also taken for all other realistic potentials. Attempts have been made to fit a large number of data points to optimize around close to 45 to 50 model parameters [22] by minimizing χ^2 per datum as the cost function.

In the traditional approach of modeling in physics, one considers only as many experimental points as the number of model parameters and then the rest of the data points are predicted. Here, we introduce a comprehensive data analysis using the later approach, wherein all possible combinations of experimental data points are considered and analyzed, to obtain the best model parameters along with uncertainties. This procedure is referred to as combinatorial data analysis (CDA).

Upon obtaining $^3S_1$ model parameters of the Morse function that fit the SPSs using CDA and a GOA, one can obtain the corresponding analytical ground-state wave function. Then, employing the simple approximation mentioned above, one can determine the D-state wave function such that the overall DWF is normalized while simultaneously giving rise to the correct quadrupole moment [23]. From the DWF, the deuteron's static properties and form factors can be determined. A detailed discussion about form factors (FFs) and related experimental data can be found in the paper by Sick [24].

Hence, the major objectives of this paper are to determine

(i) the inverse potential for the deuteron bound state using both a GOA and CDA,
(ii) the analytical DWF,
(iii) the electromagnetic form factors from an analytical DWF, and
(iv) the deuteron's static and low-energy properties.

II. METHODOLOGY

Selg [18,19] has discussed in detail a reference potential approach to obtaining inverse potentials using the Morse function, given by

$$V_M(r) = V_0\left(e^{-2(r-r_m)/a_m} - 2e^{-(r-r_m)/a_m}\right), \tag{1}$$

where the model parameters V_0 (MeV), r_m (fm), and a_m (fm) denote the depth of the potential, the equilibrium distance at which maximum attraction is felt, and the shape of the potential, respectively.

One can use a combination of Morse potentials if needed [21]. To fix three parameters of the Morse function, at least three bound states should be available. But, a deuteron has only one and hence it is not possible to fix these exactly. This is what makes the study of deuterons an extremely interesting one.

The Morse potential has certain interesting characteristics that separate it from other phenomenological potentials. They are as follows:

(i) an analytical solution of the TISE for bound states [25],
(ii) an exact analytical expression [25] of SPSs for unbound S states,
(iii) a relatively simpler wave function [25], and
(iv) shape invariance [26].

A. Morse function as a model of interaction

A strong force has been proven to exist between quarks. So, nuclear force is of a secondary nature, similar to that of van der Waals interaction in molecules. The Morse function is the most successful molecular potential that could explain various observed spectra. A deuteron in a weakly bound state can be ideally modeled as a nuclear molecule. Hence, modeling deuterons using the Morse function is appropriate.

Nuclear force is characterized by short-range repulsion, medium-range attraction, and long-range cutoff. All these features are also observed in the Morse function, thereby making it an ideal model of interaction for nuclear force.

One can observe that the Morse model has parsimony and pedagogic value. Its limitation is that it does not explicitly consider the internal interactions responsible for the obtained inverse potential. Hence, one does not have access to contributions due to central and tensor potentials that are needed for solving coupled differential equations associated with deuterons.

B. Triplet S-wave bound-state energy

The radial TISE for $\ell = 0$ (S wave) is given by

$$-\frac{\hbar^2}{2\mu}\frac{d^2u(r)}{dr^2} + V_M(r)u(r) = Eu(r), \tag{2}$$

where μ is the reduced mass of neutrons and protons. The analytical solution of the TISE is derived by Morse [27], and the ground-state energy expression is given by

$$E_0 = -\frac{\hbar^2}{2\mu a_m^2}\left(\lambda - \frac{1}{2}\right)^2, \tag{3}$$

where

$$\lambda = \sqrt{\frac{2\mu V_0 a_m^2}{\hbar^2}}. \tag{4}$$

Here, λ is called the well-depth parameter and is dependent only on V_0 and a_m.

Utilizing the experimental binding energy (BE) of the deuteron, $E_0 = -2.224\,589(22)$ MeV [28], V_0 can be expressed in terms of a_m as

$$V_0 = \frac{\hbar^2}{2\mu a_m^2}\left(0.5 + \sqrt{\frac{2\mu(2.224\,589)a_m^2}{\hbar^2}}\right)^2. \tag{5}$$

To fix the other two parameters, a_m and r_m, we utilize experimental SPSs. Out of an infinite set of values for V_0 and a_m that could give rise to an experimental BE, only one set in consonance with a particular r_m should give rise to the observed experimental SPSs. To determine the SPSs, Morse [27] suggested the phase function method.

C. Phase function method (PFM)

The Schrödinger wave equation for a particle with energy E and orbital angular momentum ℓ undergoing scattering is given by

$$\frac{\hbar^2}{2\mu}\left[\frac{d^2}{dr^2}+\left(k^2-\frac{\ell(\ell+1)}{r^2}\right)\right]u_\ell(k,r)=V(r)u_\ell(k,r), \quad (6)$$

where $k=\sqrt{E/(\hbar^2/2\mu)}$. Here, $\hbar^2/2\mu = 41.47$ MeV fm^2. The second-order differential equation, Eq. (6), has been transformed into a first-order nonhomogeneous differential equation of the Riccati type [29,30], given by

$$\frac{d\delta_\ell(k,r)}{dr} = -\frac{2\mu}{\hbar^2}\frac{V(r)}{k}[\cos[\delta_\ell(k,r)]\hat{j}_\ell(kr) - \sin[\delta_\ell(k,r)]\hat{\eta}_\ell(kr)]^2, \quad (7)$$

where $\hat{j}_\ell(kr)$ and $\hat{\eta}_\ell(kr)$ are the Ricatti-Bessel and Ricatti-Neumann functions, respectively. For $\ell=0$, $\hat{j}_0$ and $\hat{\eta}_0$ are $\sin(kr)$ and $-\cos(kr)$, respectively, and the above equation is written as

$$\frac{d\delta_0(k,r)}{dr} = -\frac{2\mu}{\hbar^2}\frac{V(r)}{k}\sin^2[kr+\delta_0(k,r)]. \quad (8)$$

The function $\delta_0(k,r)$ is called the phase function. SPSs have been obtained by numerically integrating the above equation using the Runge-Kutta (RK) fifth-order method [31] with the initial condition $\delta_0(k,r_0)=0$. The integration starts from a point close to the origin ($r=r_0$) and goes all the way up to the asymptotic region ($r=r_f$), where the interaction potential becomes zero.

The advantage of the PFM is that SPSs are directly obtained from the potential without recourse to the wave function. So, the Morse function is incorporated into the phase equation and its model parameters are optimized by using the numerical integration routine in an iterative fashion within an optimization procedure as shown in Fig. 1.

D. Optimization procedure

The procedure utilized for optimization is broadly as follows.

(i) Model parameters are given certain bounds. For example, both a_m and r_m are chosen to have values within an interval of (0, 1). We choose random values for a_m and r_m from their sample space and determine V_0 using Eq. (5).

(ii) Define a cost function that needs to be minimized. We have chosen the mean-squared error (MSE) between two data sets, given by

$$\text{MSE} = \frac{1}{N}\sum_{i=1}^{N}\left(\delta_i^{\text{expt}}-\delta_i^{\text{sim}}\right)^2, \quad (9)$$

where δ_i^{sim} are SPSs obtained using the PFM solved via the RK fifth-order method and δ_i^{expt} are experimental SPSs from the mean-energy partial-wave analysis data (MEPWAD) of the Granada Group [22].

(iii) Use the optimization routine to determine the best parameters that fit the experimental data with a minimum MSE.

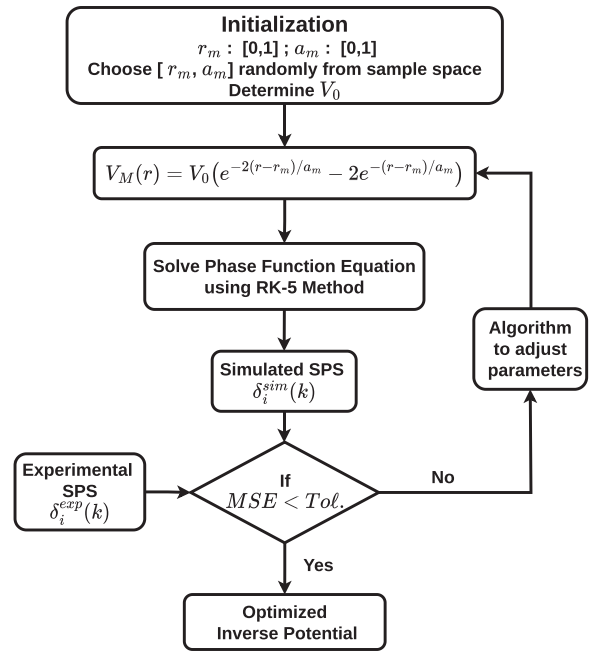

FIG. 1. Flow chart for the PFM in tandem with variational Monte Carlo technique as an optimization procedure.

The detailed procedure for obtaining the final optimized parameters using CDA is discussed in Sec. III and separately provided in the Supplemental Data [32]. Once the model parameters are obtained, one can determine the analytical DWF.

E. Deuteron ground-state wave function

To determine deuteron charge and magnetic FFs, measured from electron scattering experiments, knowledge of the ground-state wave function is a basic requirement. The analytical solution for the ground-state wave function due to the Morse potential [27] is given by

$$u_0(z) = N_0 e^{-z/2}z^{\epsilon_0},\ z(r) = 2\lambda e^{-(r-r_m)/a_m}, \quad (10)$$

where

$$\epsilon_0 = \sqrt{\frac{2\mu E_0 a_m^2}{\hbar^2}} \quad (11)$$

and N_0 is determined from normalization of the DWF $\psi_D(r)$. Considering the $^3D_1$ wave function $w_2(r)$ to be proportional to

$u_0(r)$ [17,33], N_0 has been determined such that

$$\int_0^\infty |\psi_D(r)|^2 r^2 dr = \int_0^\infty \left[u_0^2(r) + w_2^2(r)\right] dr = 1. \quad (12)$$

$^3S_1$ and $^3D_1$ wave functions with relative normalization are as follows:

$$u_0(z) = C_0 e^{-z/2} z^{\epsilon_0},\ C_0 = \sqrt{\frac{(2a-1)P_S}{a_m \Gamma(2a)}},\ a = \sqrt{\frac{2\mu V_0 a_m^2}{\hbar^2}}, \quad (13)$$

$$w_2(z) = C_2 e^{-z/2} z^{\epsilon_0},\ C_2 = \sqrt{\frac{(2a-1)P_D}{a_m \Gamma(2a)}}. \quad (14)$$

It should be noted that Eq. (12) has two unknowns and, hence, one more condition needs to be utilized to fix them. This is done by choosing one of the static properties of deuterons from experimental data, typically, the electric quadrupole moment [2]. Considering relativistic effects and the deuteron's finite size to be negligible, the quadrupole moment is given by following expression:

$$Q_D = \frac{1}{20} \int_0^\infty r^2 \left(\sqrt{8} u_0(r) w_2(r) - w_2^2(r)\right) dr. \quad (15)$$

F. Emergent deuteron properties

Once the DWF is determined, one can determine both static properties and FFs.

1. Static properties of a deuteron

Static properties like the matter radius (r_{Dm}), the charge radius ($r_{\rm ch}$), and the magnetic moment (μ_D) can be determined using the following expressions [1,34]:

$$r_{Dm}^2 = \frac{1}{4} \int_0^\infty r^2 \left[u_0^2(r) + w_2^2(r)\right] dr, \quad (16)$$

$$r_{\rm ch}^2 = r_{Dm}^2 + \Delta r_m^2 + r_p^2 + r_n^2 + \frac{3}{4}\left(\frac{\hbar}{m_p}\right)^2, \quad (17)$$

and

$$\mu_D = \mu_s - 1.5(\mu_s - 0.5) P_d, \quad (18)$$

where $r_p = 0.862(12)$ fm is the charge rms radius of the proton, ${r_n}^2 = -0.113(5)$ fm^2 is charge rms radius of the neutron, and $\Delta r_m^2 = \pm 0.01$ fm^2, and P_D is the D-state probability.

2. Deuteron form factors

To understand the nucleon's structure, the study of measurable fundamental quantities such as electromagnetic FFs is of paramount importance. The FFs are helpful in describing the spatial variation of the distribution of the magnetization and charge of the nucleons within a two-nucleon bounded system. A deuteron cannot be considered a pointlike object. Hence, an electron-deuteron (e-D) elastic-scattering process is utilized to probe the structure of the nucleus to obtain FFs.

In nonrelativistic theory, without considering $(v/c)^2$ corrections, the following relations are used for calculations of electromagnetic FFs as functions of the four-momentum Q value:

$$F_C(Q) = \left[G_{E_p} + G_{E_n}\right] \int_0^\infty \left[u_0^2 + w_2^2\right] j_0 dr, \quad (19)$$

$$F_Q(Q) = \frac{2}{\zeta}\sqrt{\frac{9}{8}}\left[G_{E_p} + G_{E_n}\right] \int_0^\infty \left[u_0 w_2 - \frac{w_2^2}{\sqrt{8}}\right] j_2 dr, \quad (20)$$

$$F_M(Q) = 2\left[G_{M_p} + G_{M_n}\right] \int_0^\infty \left[\left(u_0^2 - \frac{w_2^2}{2}\right) j_0\right] dr + 2\left[GM_p + G_{M_n}\right] \int_0^\infty \left[\left(\frac{u_0 w_2}{\sqrt{2}} + \frac{w_2^2}{2}\right) j_2\right] dr + \frac{3}{2}\left[G_{E_p} + G_{E_n}\right] \int_0^\infty w_2^2 [j_0 + j_2] dr, \quad (21)$$

where j_0 and j_2 are spherical Bessel functions with an argument $(Qr/2)$. While G_{E_p} and G_{E_n} are proton and neutron isoscalar electric FFs, G_{M_p} and G_{M_n} are corresponding isoscalar magnetic FFs. The factor ζ is related to the four-momentum transfer Q value by

$$\zeta = \frac{Q^2}{4M_D^2}, \quad M_D = 1875.63\ \text{MeV}.$$

Here, the charge FF for the neutron G_{E_n} is assumed to be zero as in Ref. [18] and the charge FF for the proton G_{E_p} is parametrized using the following dipole FF relation:

$$G_{E_p} = \frac{1}{(1 + 0.054\,844 Q^2)^2}. \quad (22)$$

The magnetic FF for the nucleon is determined using the following:

$$G_{M_p} = \mu_p G_{E_p} \quad \text{and} \quad G_{M_n} = \mu_n G_{E_p},$$

where $\mu_p = 2.7928$ and $\mu_n = -1.9130$ are the magnetic moments of the proton and the neutron given in units of nuclear magnetons. We have determined all three FFs directly by integrating the deuteron's analytical wave function. Here it is to be noted that, within nonrelativistic limits, a nucleon electric FF contributes to the deuteron's charge as well as to the quadrupole structure, while the other two FFs contribute to the magnetic structure of the deuteron. We can then calculate deuteron structure functions, $A(Q)$ and $B(Q)$. These are related to three electromagnetic FFs due to charge $F_C(Q)$, quadrupole $F_Q(Q)$, and magnetic $F_M(Q)$, through the following [35–44]:

$$A(Q) = F_C^2 + \frac{8}{9}\zeta^2 F_Q^2 + \frac{2}{3}\zeta F_M^2, \quad (23)$$

$$B(Q) = \frac{4}{3}\zeta(1+\zeta) F_M^2. \quad (24)$$

Using $A(Q)$ and $B(Q)$ yields the unpolarized e-D elastic-scattering cross section given by the following relation [2,45]:

$$\frac{d\sigma}{d\Omega} = \frac{\sigma_{\rm Mott}}{1 + \frac{2E}{M_d}\sin^2\left(\frac{\theta_e}{2}\right)} [A(Q) + B(Q)\tan^2(\theta_e/2)], \quad (25)$$

where $\sigma_{\rm Mott}$ is the Mott cross section, given as

$$\sigma_{\rm Mott} = \alpha^2 E' \cos^2(\theta_e/2)/[4E^3 \sin^4(\theta_e/2)].$$

TABLE I. Optimized parameters for the $^3S_1$ state using the GOA and CDA. In the latter case, parameter values consisting of extreme depths are shown. The scattering length (a in fm) and the effective range (r_e in fm) are obtained, using SPSs determined from these optimized parameters. Their corresponding experimental values [47] are given in curly brackets.

Analysis	$[V_0, r_m, a_m]$	MAE	a (fm)	r_e (fm)
GOA	[114.153, 0.841, 0.350]	0.35	5.35(1) {5.424(3)}	1.75(2) {1.760(5)}
CDA	[93.577, 0.843, 0.394]	1.1	5.38(2)	1.76(1)
	[116.382, 0.843, 0.346]	0.4		

Here, Q (fm^{-1}) is the momentum transfer, $\alpha = e^2/4\pi = 1/137$ is the fine-structure constant, θ_e is the electron scattering angle, E and E' are the electron's incident and final scattered energies, and M_D is the deuteron's mass.

III. RESULTS, ANALYSIS, AND DISCUSSION

The experimental MEPWAD for SPSs for the $^3S_1$ state have been taken from Arriola *et al.*, the Granada group [22]. These data consist of SPSs for laboratory energies ranging from 1 to 350 MeV, given by the set [1, 5, 10, 25, 50, 100, 150, 200, 250, 300, 350]. Because scattering parameters depend upon low-energy data, it is important to include experimental SPSs at low energy. Hence, $[E, \delta]$ given by [0.1, 169.32] for the $^3S_1$ data point from Arndt [46] has been added.

A. Overall data fitting using the global optimization algorithm

Initially, model parameters are optimized by choosing to minimize the MSE for the entire data set consisting of 12 points. For triplet ground-state $^3S_1$, only two parameters, a_m and r_m, are varied and V_0 is calculated via the energy constraint, Eq. (5). The optimized values obtained are shown in Table I. The MSE values obtained are < 0.1, and to quantify the performance, we have chosen the mean absolute error (MAE) as a measure. The triplet SPS has been obtained with a MAE of 0.35.

The uncertainties, $\Delta\delta(E)$, in the SPS data at different energies specified in the Granada Group's MEPWAD [22], have been utilized to create two extreme data sets. One by adding $\Delta\delta(E)$ to $\delta(E)$ and the other by subtracting $\Delta\delta(E)$ from $\delta(E)$. The model parameters obtained are as follows:

$^3S_1$: [116.040, 0.832, 0.347] and [112.306, 0.850, 0.354].

These model parameter sets are used to obtain uncertainties in SPSs for the triplet state. While the obtained SPSs are utilized to determine the low-energy scattering parameters, the model parameters give rise to the DWF from which various static properties are determined. The DWF also helps in the calculation of the deuteron's various electromagnetic form factors.

This kind of analysis is akin to data fitting in the machine-learning paradigm, which we denoted as the GOA, wherein best parameters are obtained by including all available experimental values, at the validation stage, to obtain model interaction. One should be aware that there is a good possibility that the GOA might lead to overfitting [24]. Also, optimized parameters could be sensitive to the data set. This aspect is being studied.

1. Scattering phase shifts

The SPSs for $^3S_1$ obtained with the GOA are shown in Fig. 2 using a bold line. The corresponding interaction potential is shown in the inset of Fig. 2. The variations in SPSs and certain widths seen in Fig. 2 are due to the uncertainties in the model parameters calculated using CDA (see Sec. III 2). The uncertainties due to extreme data sets discussed above are within those from CDA and hence are not separately shown. SPSs for all higher ℓ channels are also found to match well with experimental data (to be communicated separately).

2. Low-energy scattering and static properties of deuterons

Low-energy parameters, scattering length (a) and effective range (r_e), have been obtained for the S wave by plotting graphs of $kcot(\delta)$ vs k. The slope and the intercept give rise to a and r_e. The results are compared alongside experimental ones, given in curly brackets, in the upper half of Table I. Once again, extreme data sets for model parameters were utilized to present uncertainties for low-energy properties in Table I.

The $^3S_1$ ground-state wave function $u_0(r)$ has been determined by substituting model parameters in Eq. (10) and is shown in Fig. 3(a). The $^3D_1$ wave function $w_2(r)$, also shown in Fig. 3(a), has been determined so as to ensure normalization and the correct electric quadrupole moment value of 0.2589 fm^2. The parameters for generating analytical wave functions for $^3S_1$ and $^3D_1$ of deuterons, using Eqs. (13) and (14), respectively, are given in Table II. The value of $P_D = 2.05$ is comparatively much less than what has been obtained by

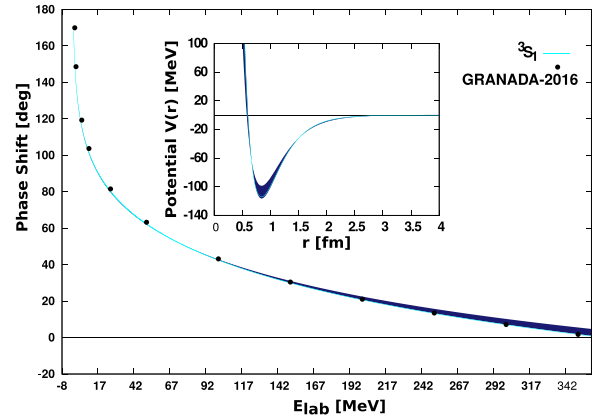

FIG. 2. Triplet scattering phase shifts at laboratory energies compared with experimental MEPWAD [22]. The interaction potentials were obtained using CDA and are shown in the inset. The bold lines are best fits obtained using the GOA.

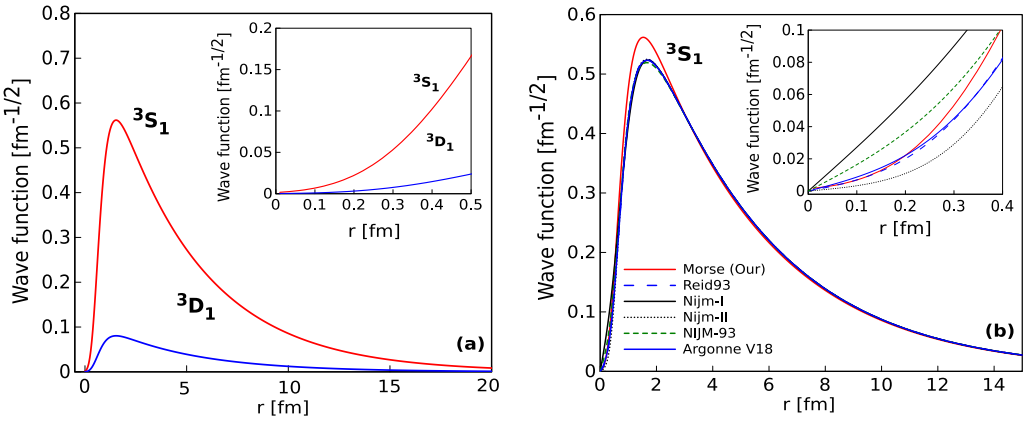

FIG. 3. (a) Analytical deuteron wave function for $^3S_1$ and $^3D_1$ states. Inset shows variations of wave functions closer to the origin. (b) Ground-state wave function in comparison with other high-precision potentials. The inset shows variations closer to the origin.

various precision potentials [7]. On the other hand, it is of a value similar to that obtained using SUSY methodology [17], which is 1.89, that has the same approximation as ours. Due to the repulsive nuclear core, the wave functions can be seen to be dropping sharply near the origin, while peaks for $u_0(r)$ and $w_2(r)$ occur in the intermediate range ($1 \leqslant r \leqslant 2$ fm).

A comparative plot of $^3S_1$ wave functions obtained from various realistic potentials that typically utilize the one-pion-exchange potential (OPEP) as part of their ansatz for large r values ($>$ 2–3 fm) is shown in Fig. 3(b). One can observe in the inset of the figure that our analytical wave function has a close match with that of the Argonne v_{18} potential for very small r values ($\leqslant 0.25$ fm) and it raises to a higher peak than the rest of the wave functions in the intermediate region. It should be emphasized that our analytical wave function for $^3S_1$ matches the expected variation for the asymptotic region beyond ($r > 4$ fm) that expected from the OPEP exactly. So, the Morse potential interaction is an ideal mathematical representation that is able to effectively include within its tail the observed success of the OPEP for a large range.

The average values of S-state and D-state probabilities, P_S and P_D, are 98% and 2%, respectively. The rest of the static properties, such as the magnetic moment, the matter radius, and the charge radius, have been determined, along with their uncertainties, and are presented in Table III.

B. Combinatorial data analysis in physics modeling

In principle, for modeling in a physics context, one would expect that the number of data points to be chosen for optimization should be equal to the number of model parameters. If the number of data points chosen is larger than the number of model parameters, then the system of equations is overdetermined or else it is underdetermined. Either way, it does not have a unique solution. The obtained parameters must be able to explain the rest of the data reasonably well. Then, a question arises as to what would be the right way to choose 2 data points from among the 12 available for the triplet state. This would result in a total of $^{12}C_2(= 66)$ combinations. Initially, we have obtained optimized parameters for each of these available combinations and then carefully analyzed the results. Here, are some important observations.

(i) The depth of the potential is energy dependent. That is, data points from low-energy regions [0.1, 25] have resulted in lower V_0 values as compared to those from higher-energy regions [200, 350].
(ii) The model has good predictive power for interpolated data points but errors increase due to extrapolation, especially at far away points.

For instance, considering data points from the low-energy region [0.1, 10] has resulted in better prediction of SPSs for data points in the intermediate range [25, 150] as compared to those in the high-energy region [200, 350], where the SPSs obtained had comparatively larger errors. Similarly, considering two data points in the high-energy region [200, 350] for optimization has resulted in poor accuracy in scattering parameter values, reflecting that the SPSs of the low-energy region, important for calculating the scattering length and the effective range, have not been determined to good accuracy.

Based on these observations, the MAE was utilized as a quantitative measure. After carefully analyzing the results at various stages of our calculations for all possible combinations, we have applied the following criteria: In the first step, for fixing the r_m value, we have considered those combinations for which MAE $\leqslant 2$. Then, in second step, scattering and static properties as well as SPSs were obtained for each of the combinations, with MAE $\leqslant 1$, and their averages and standard deviations were determined and tabulated. This is the procedure for CDA, performed at the validation stage of our model.

Analysis of the $^3S_1$ state. Keeping in mind that ground-state energy is retained in the case of $^3S_1$, through Eq. (5), it is expected that one should obtain an equilibrium value for r_m

TABLE II. Parameters for generating $^3S_1$ and $^3D_1$ analytical wave functions of deuterons as shown in Fig. 3.

ϵ_0	a	C_0 (fm$^{-1/2}$)	C_2 (fm$^{-1/2}$)	P_S (%)	P_D (%)
0.0811	0.5807	0.6972	0.1002	97.95	2.05

TABLE III. Static properties for deuterons calculated using the Morse potential in comparison with experimental values taken from Ref. [2] and others [17,45].

	Expt.	Our			
Quantity	[2]	CDA	GOA	[17]	[45]
μ_D (μ_N)	0.8574	0.8687(1)	0.8683(1)	0.8690[a]	0.8519(72)
r_{Dm} (fm)	1.975(3)	1.9537(39)	1.9285(44)	1.975 07(78)	1.953 20(475)
$r_{\rm ch}$ (fm)	2.130(10)	2.1088(36)	2.1037(41)	2.125 62(78)	2.1354(9)

[a]This value was calculated using P_D given in Ref. [45].

while determining the SPS. It was observed that out of 66 combinations of a_m and r_m, 64 of them resulted in MAE $\leqslant 2$, which gave $r_m = 0.843 \pm 0.013$ fm. Once the r_m value is fixed, there is only one parameter, a_m, that needs to be determined. Hence, only one energy data point is required to determine a_m. That is, a total of 12 values will be obtained for a_m from which the corresponding V_0 values shall be determined to a required accuracy such that the energy is retained to 6 decimal places. The resultant model parameters shown in Table I (third column) correspond to combinations giving rise to two extreme potential depths. It was found that all 12 combinations resulted in MAE $\leqslant 1$. Hence, all of them are considered for determining final properties. The electric quadrupole moment (Q_D) is retained in all calculations to obtain the appropriate $w_2(r)$. Then, the magnetic moment (μ_D) and the matter radius (r_{Dm}) are determined for each combination. The averages along with their uncertainties given in Table III are found to be very close to expected experimental values and comparable to those obtained using realistic precision potentials. The $^3S_1$ SPSs with uncertainties and corresponding interaction potentials, with shaded regions covering all possible depths, are shown in Fig. 2. These were also considered while determining various deuteron form factors.

C. Deuteron form factors

The analytical wave functions $u_0(r)$ and $w_2(r)$ have been directly used in integrals, in Eqs. (20)–(22), to determine electromagnetic FFs, $F_C(Q)$, $F_Q(Q)$, and $F_M(Q)$, respectively. The integral calculations are performed using symbolic PYTHON. These are plotted in Figs. 4–6. One can see good agreement with experimental data [35–44] for lower momentum transfer Q values up to 3–4 fm^{-1} after which our values slowly deviate from the expected. As $Q \to 0$ (static moments), values of all three FFs obtained (experimental values shown in parentheses are from Ref. [2]) are as follows,

$$F_C(Q \to 0) = 1.0(\mathbf{1.0}),$$
$$F_M(Q \to 0) = 1.7714(\mathbf{1.7148}),$$
$$F_Q(Q \to 0) = 24.97 - 27.56(\mathbf{25.83}),$$

and can be seen to be in good agreement with the experimental values. While various realistic potentials always give a value for $F_Q(0)$ below 25.83 [2], it falls well within the range provided by our CDA approach.

In the case of $F_C(Q)$, experimental data are available from nearly 1 fm^{-1} to about 7 fm^{-1} from different papers. Both Abbot *et al.*'s compiled data [37] (0.86–6.64 fm^{-1}) and Nikolenko *et al.*'s data [42] ($Q = 2.9$–4.6 fm^{-1}) indicate an upward trend. While Garcon *et al.*'s data [43] ($Q = 0.988$–4.62 fm^{-1}) do not capture the upward trend beyond 4 fm^{-1}, both leading order (LO) and next-to-next-to-next-to-leading order (N3LO) calculations [48] capture experimental trends occurring just before 4 fm^{-1}. While the former matches Nikolenko *et al.*'s trend [42], the latter one shows closeness to Abbot *et al.*'s data [37]. Our analysis, as seen in Fig. 4, shows an upward trend to be occurring closer to 5 fm^{-1} and our data beyond 5 fm^{-1} fall below experimental values. In the case of $F_Q(Q)$, all available experimental data [38,43,44] have a similar trend. Both LO and N3LO calculations match our values of $F(Q)$ at $Q \approx 0$. LO calculations match experimental data for Q values up to 4.62 fm^{-1}. For values beyond this, the trend of LO calculations is downward as compared to the experimental data of Abbot *et al.* [37]. On the other hand, N3LO calculations are slightly below experimental data from Nikolenko *et al.* [42] and Abbot *et al.* [37] and capture Garcon data better for Q values up to 3.78 fm^{-1}. Beyond this N3LO calculations bend farther away from both LO calculations and experimental data. Our analysis, as seen in Fig. 5, lies below experimental data for Q values up to 4.62 fm^{-1} but correctly obtains values for $Q = 6.15$ and 6.64 fm^{-1}. In the case of $F_M(Q)$, Garcon *et al.* [43] ($Q = 0.988$–4.62 fm^{-1}) captures in essence trends from both

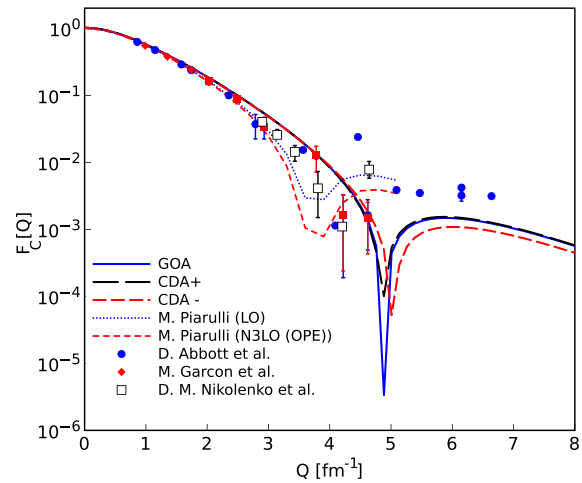

FIG. 4. Deuteron form factor F_C as a function of Q (fm^{-1}). Experimental data are taken from different experimental works [34–43]. LO and N3LO calculations have been taken from Ref. [47] for comparison.

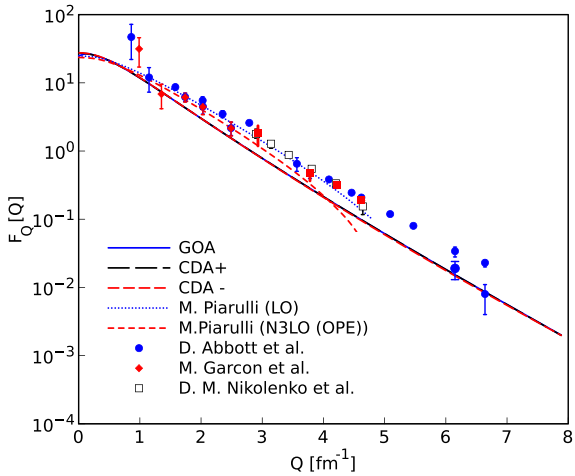

FIG. 5. Deuteron form factor F_Q as a function of Q (fm^{-1}). Experimental data are taken from different experimental works [34–43]. Leading order (LO) and N3LO calculations have been taken from Ref. [47] for comparison.

Ganichot *et al.* [39] ($Q = 0.68$–2.43 fm^{-1}) and Auffret *et al.* [36] ($Q = 2.59$–5.28 fm^{-1}). While LO and N3LO calculations suggest a dip at around 4.5 fm^{-1}, experimental data do not show such a trend. Our analysis, as seen in Fig. 6, correctly matches up to 3.5 fm^{-1} and then slowly tends to go farther as Q increases and indicates a dip at around 5.5 fm^{-1}. Next, these three electromagnetic FFs in turn are used in Eqs. (23) and (24) to obtain the structure form factor functions $A(Q)$ and $B(Q)$, shown in Figs. 7(a) and 7(b), respectively. Our results of the deuteron's electric A_Q and magnetic B_Q structure functions are in quite good agreement with the experimental data [35–37,39–42,44].

In the case of $A(Q)$, the experimental data covers from around 0.01 to 10 fm^{-1} according to various experimental

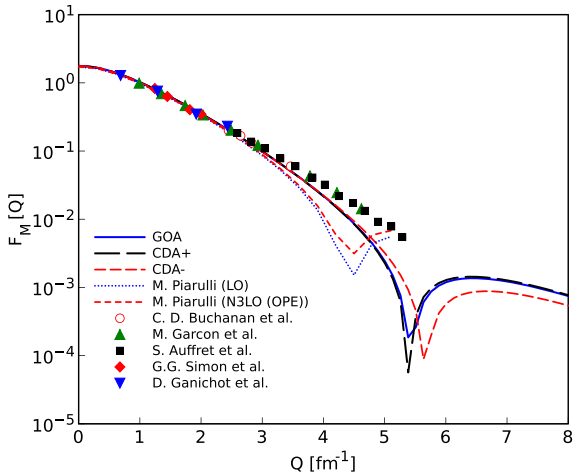

FIG. 6. Deuteron form factor F_M as a function of Q (fm^{-1}). Experimental data are taken from different experimental works [34–43]. Leading order (LO) and N3LO calculations have been taken from Ref. [47] for comparison.

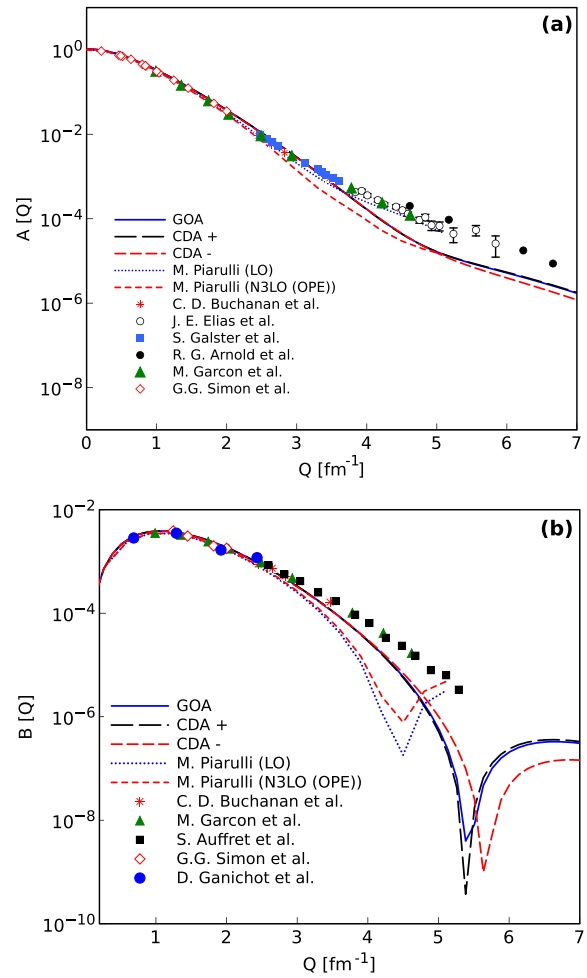

FIG. 7. Deuteron (a) electric $A(Q)$ and (b) magnetic $B(Q)$ structure function variations with Q (fm^{-1}). Experimental values are taken from Refs. [34–36,38–41,43]. Leading order (LO) and N3LO calculations have been taken from Ref. [47] for comparison.

works from Simon *et al.* [38] ($Q = 1.24$–2 fm^{-1}), Garcon *et al.* [43] ($Q = 0.988$–4.62 fm^{-1}), Galster *et al.* [35] ($Q = 2.48$–3.61 fm^{-1}), Elias *et al.* [34] ($Q = 3.83$–5.84 fm^{-1}), and Arnold *et al.* [41] ($Q = 4.61$–10.04 fm^{-1}). LO calculations show experimental trends all the way up to 5 fm^{-1} and may correctly show higher values upon extension. N3LO calculations, on other hand, match experimental data only up to 2 fm^{-1} and then increasingly fall short with increasing Q. The experimental data for $B(Q)$ are from Ganichot *et al.* [39] ($Q = 0.68$–2.43 fm^{-1}), Garcon *et al.* [43] ($Q = 0.988$–4.62), Simon *et al.* [38] ($Q = 1.24$–2 fm^{-1}), and Auffret *et al.* [36] ($Q = 2.59$–5.28 fm^{-1}). All data more or less show a similar trend. While LO and N3LO calculations correctly follow values up to 3 fm^{-1}, for points beyond they are way lower. Also, they tend to predict a dip at about 4.5 fm^{-1}. On the other hand, our analysis, as seen in Fig. 7(b), not only matches with experimental values up to 3 fm^{-1} but is closer for points beyond 3 fm^{-1} as well. We predict a dip at around 5.5 fm^{-1}, after which the $B(Q)$ value again increases.

IV. CONCLUSIONS

The molecular Morse interaction has been shown to be an ideal phenomenological potential to describe the observed structure and form factors of deuterons. It not only retains experimental ground-state energy along with correctly predicting observed scattering phase shifts for laboratory energies up to 350 MeV but also gives an analytical wave function for the $^3S_1$ state that matches the asymptotic wave function expected from the OPEP perfectly.

The real take away of this entire exercise is the simplicity of the chosen model interaction which has a single mathematical function that represents the potential over the entire range of nuclear force. All other realistic potentials model the nuclear force using different mathematical functions for short and intermediate ranges and chose OPE-type potentials for long range. The advantage of the Morse function is that it has a tail that is dictated by the shape factor a_m that has been adjusted to obtain SPSs and it is seen to be able to effectively match the expected OPEP variation.

Another important contribution is that we have provided a range for model parameters by determining uncertainties by using combinatorial data analysis, which we think is a unique procedure developed by us for solving the np system. The advantage of giving a range for model parameters is that it allows us to determine the nuclear binding energies with their corresponding uncertainties. This is not possible with most of the existing realistic potentials. This point has been emphasized by the Granada Group [22]. Second, this approach is very apt from a physics modeling point of view, as compared to data-fitting strategies, which are more akin to a machine-learning paradigm.

Also, parsimony is one of the important goals of a good hypothesis in scientific research. When there exists an analytical ground-state wave function that is able to aptly describe various deuteron form factors, it would be unnecessary to deal with large data sets, in the form of tables, to represent it. It has been shown by Zhaba in Refs. [48,49] and references therein, and is also well known in computational physics, that numerical techniques tend to accumulate errors with increasing numbers of evaluations. Further, some of the realistic potentials, such as CD-Bonn and Moscow, have been observed to have knots in their component wave functions, near the origin, which implies inconsistencies and inaccuracies in their numerical procedures [50].

Finally, the Morse function is pedagogically the easiest potential whose time-independent Schrodinger equation can be solved analytically for both the ground state and the scattering S state, which have maximum contributions to the total scattering cross section at low energies up to 50 MeV. We have shown that the Morse function can reasonably explain all the deuteron's experimental observables from low-energy scattering and static properties to its various electromagnetic form factors. Our results for higher ℓ channels are worked out and have very good agreement for all energies up to 350 MeV. The contributions due to p-h channels significantly improve calculations of total scattering cross sections and accurately describe the observed experimental data for all energies up to 350 MeV and will be communicated elsewhere. This approach has features that could result in better understanding of NN interaction and in turn validate or clarify the underlying mechanism that is still unclear from varied theoretical constructs of existing realistic potentials.

The authors declare that they have no conflicts of interest.

[1] V. I. Zhaba, arXiv:1706.08306.
[2] M. Garcon and J. W. Van Orden, in *Advances in Nuclear Physics*, edited by J. W. Negele and E. W. Vogt (Springer, Boston, 2001), Vol. 26, pp. 293–378.
[3] R. Machleidt, Phys. Rev. C **63**, 024001 (2001).
[4] R. V. Reid, Jr., Ann. Phys. (NY) **50**, 411 (1968).
[5] V. I. Kukulin, V. N. Pomerantsev, and A. Faessler, A. J. Buchmann, and E. M. Tursunov, Phys. Rev. C **57**, 535 (1998).
[6] M. Lacombe, B. Loiseau, J. M. Richard, R. V. Mau, J. Côté, P. Pirès, and R. de Tourreil, Phys. Rev. C **21**, 861 (1980).
[7] R. B. Wiringa, V. G. J. Stoks, and R. Schiavilla, Phys. Rev. C **51**, 38 (1995).
[8] V. G. J. Stoks, R. A. M. Klomp, C. P. F. Terheggen, and J. J. de Swart, Phys. Rev. C **49**, 2950 (1994).
[9] A. Pich, Rep. Prog. Phys. **58**, 563 (1995).
[10] M. Naghdi, Phys. Part. Nucl. **45**, 924 (2014).
[11] R. Machleidt, Phys. Rep. **242**, 5 (1994).
[12] M. Naghdi, Phys. Part. Nucl. Lett. **11**, 410 (2014).
[13] H. Yukawa, S. Sakata, M. Kobayasi, and M. Taketani, Prog. Theor. Phys. Suppl. **1**, 46 (1955).
[14] R. A. Malfliet and J. A. Tjon, Nucl. Phys. A **127**, 161 (1969).
[15] J. Bhoi and U. Laha, Braz. J. Phys. **46**, 129 (2016).
[16] B. Khirali, A. K. Behera, J. Bhoi, and U. Laha, Ann. Phys. (NY) **412**, 168044 (2020).
[17] T. Koohrokhi and S. Kartal, Commun. Theor. Phys. **74**, 075301 (2022).
[18] M. Selg, Proc. Est. Acad. Sci. **65**, 267 (2016).
[19] M. Selg, Mol. Phys. **104**, 2671 (2006).
[20] A. Khachi, L. Kumar, and O. S. K. S. Sastri, Phys. At. Nucl. **85**, 382 (2022).
[21] O. S. K. S. Sastri, A. Khachi, and L. Kumar, Braz. J. Phys. **52**, 58 (2022).
[22] R. N. Perez, J. E. Amaro, and E. R. Arriola, J. Phys. G: Nucl. Part. Phys. **43**, 114001 (2016).
[23] T. E. Ericson and M. Rosa-Clot, Nucl. Phys. A **405**, 497 (1983).
[24] I. Sick, Prog. Part. Nucl. Phys. **47**, 245 (2001).
[25] A. Matsumoto, J. Phys. B: At., Mol. Opt. Phys. **21**, 2863 (1988).
[26] D. A. Morales, Chem. Phys. Lett. **394**, 68 (2004).
[27] P. M. Morse, Phys. Rev. **34**, 57 (1929).
[28] G. L. Greene, E. G. Kessler, Jr., R. D. Deslattes, and H. Borner, Phys. Rev. Lett. **56**, 819 (1986).
[29] V. Babikov, Sov. Phys. Usp. **10**, 271 (1967).
[30] F. Calogero, *Variable Phase Approach to Potential Scattering* (Academic, New York, 1967).

[31] J. C. Butcher, in *Proceedings of the Conference on the Numerical Solution of Differential Equations* (Springer, Berlin, Heidelberg, 1969).
[32] See Supplemental Material at http://link.aps.org/supplemental/10.1103/PhysRevC.107.064002 for obtaining final optimized parameters using combinatorial data analysis.
[33] A. F. Nicholson, Aust. J. Phys. **15**, 169 (1962).
[34] J. E. Elias, J. I. Friedman, G. C. Hartmann, H. W. Kendall, P. N. Kirk, M. R. Sogard, L. P. Van Speybroeck, and J. K. De Pagter, Phys. Rev. **177**, 2075 (1969).
[35] S. Galster, H. Klein, J. Moritz, K. H. Schmidt, D. Wegener, and J. Bleckwenn, Nucl. Phys. B **32**, 221 (1971).
[36] S. Auffret, J. M. Cavedon, J. C. Clemens, B. Frois, D. Goutte, M. Huet, P. Leconte, J. Martino, Y. Mizuno, X. H. Phan, S. Platchkov, and I. Sick, Phys. Rev. Lett. **54**, 649 (1985).
[37] D. Abbott, A. Ahmidouch, H. Anklin, J. Arvieux, J. Ball, S. Beedoe, E. J. Beise, L. Bimbot, W. Boeglin, H. Breuer, and R. Carlini, Eur. Phys. J. A **7**, 421 (2000).
[38] G. G. Simon, C. Schmitt, and V. H. Walther, Nucl. Phys. A **364**, 285 (1981).
[39] D. Ganichot, B. Grossetête, and D. B. Isabelle, Nucl. Phys. A **178**, 545 (1972).
[40] C. D. Buchanan and M. R. Yearian, Phys. Rev. Lett. **15**, 303 (1965).
[41] R. G. Arnold, B. T. Chertok, E. B. Dally, A. Grigorian, C. L. Jordan, W. P. Schutz, R. Zdarko, F. Martin, and B. A. Mecking, Phys. Rev. Lett. **35**, 776 (1975).
[42] D. M. Nikolenko, H. Arenhovel, L. M. Barkov, S. L. Belostotsky, V. F. Dmitriev, M. V. Dyug, R. Gilman, R. J. Holt, L. G. Isaeva, C. W. de Jager, E. R. Kinney, R. S. Kowalczyk, B. A. Lazarenko, A. Y. Loginov, S. I. Mishnev, V. V. Nelyubin, A. V. Osipov, D. H. Potterveld, I. A. Rachek, R. S. Sadykov *et al.*, Phys. Rev. Lett. **90**, 072501 (2003).
[43] M. Garçon, J. Arvieux, D. H. Beck, E. J. Beise, A. Boudard, E. B. Cairns, J. M. Cameron, G. W. Dodson, K. A. Dow, M. Farkhondeh, H. W. Fielding, J. B. Flanz, R. Goloskie, S. Hoibraten, J. Jourdan, S. Kowalski, C. Lapointe, W. J. McDonald, B. Ni, L. D. Pham *et al.*, Phys. Rev. C **49**, 2516 (1994).
[44] N. Takigawa and K. Washiyama, *Fundamentals of Nuclear Physics* (Springer, Berlin, 2017), p. 80.
[45] B. Rezaei and A. Dashtimoghadam, J. Theor. Appl. Phys. **8**, 203 (2014).
[46] R. A. Arndt (private communication).
[47] M. Piarulli, L. Girlanda, L. E. Marcucci, S. Pastore, R. Schiavilla, and M. Viviani, Phys. Rev. C **87**, 014006 (2013).
[48] V. I. Zhaba, arXiv:1603.05382.
[49] V. I. Zhaba, World Sci. News **129**, 255 (2019).
[50] V. I. Zhaba, Mod. Phys. Lett. A **31**, 1650139 (2016).